
BEVDepth: Acquisition of Reliable Depth for Multi-view 3D Object Detection

Yinhao Li¹ Zheng Ge¹ Guanyi Yu¹ Jinrong Yang^{1,2}
Zengran Wang¹ Yukang Shi^{1,3} Jianjian Sun¹ Zeming Li¹
¹Megvii Inc. (Face++), ²Huazhong University of Science and Technology,
³Xi'an Jiaotong University
{liyinhao, gezheng, yuguanyi, yangjinrong, wangzengran,
shiyukang, sunjianjian, lizeming}@megvii.com

Abstract

In this research, we propose a new 3D object detector with a trustworthy depth estimation, dubbed BEVDepth, for camera-based Bird’s-Eye-View (BEV) 3D object detection. By a thorough analysis of recent approaches, we discover that the depth estimation is implicitly learned without camera information, making it the de-facto fake-depth for creating the following pseudo point cloud. BEVDepth gets explicit depth supervision utilizing encoded intrinsic and extrinsic parameters. A depth correction sub-network is further introduced to counteract projecting-induced disturbances in depth ground truth. To reduce the speed bottleneck while projecting features from image-view into BEV using estimated depth, a quick view-transform operation is also proposed. Besides, our BEVDepth can be easily extended with input from multi-frame. Without any bells and whistles, BEVDepth achieves the new state-of-the-art 60.0% NDS on the challenging nuScenes test set while maintaining high efficiency. For the first time, the performance gap between the camera and LiDAR is largely reduced within 10% NDS.

1 Introduction

Due to its high efficiency and rich semantic information, camera-based 3D object detection has drawn a lot of interest, especially in the field of autonomous driving. Recent vision-based techniques [1, 2, 3] rely mostly on pixel-wise depth estimation given the images from numerous cameras. A view-transform sub-network is then added to project the feature from the image view into the bird’s-eye view alongside intrinsic and extrinsic information. Despite the popularity of these depth-based 3D detectors, it is natural to ask: *what is the quality and efficiency of the depth estimation within these detectors? Does it meet the requirement for precise and effective 3D object detection?*

In this paper, we first provide a quantitative and qualitative analysis of depth estimation. The correlation between the actual and predicted depth of BEVDet [1] is shown in Fig. 1(a). Though the outcomes of 3D detection are respectable, we find that the accuracy of depth estimation is surprisingly inadequate. Such a poor depth perception inspires us to investigate what effect better depth has on 3D detection. We thus replace the predicted depth in BEVDet during view-transformation with depth ground-truth generated from point clouds. Results in Fig. 1(c) show that adopting ground-truth depth boosts mAP and NDS by 18.8% and 18.2%, respectively. Moreover, the translation error is greatly reduced from 0.750 to 0.393. Such a phenomenon reveals the quality of intermediate depth is the key to improving multi-view 3D object detection.

Recall of the depth-based 3D detector [1, 2, 3], we have the following empirical knowledge:

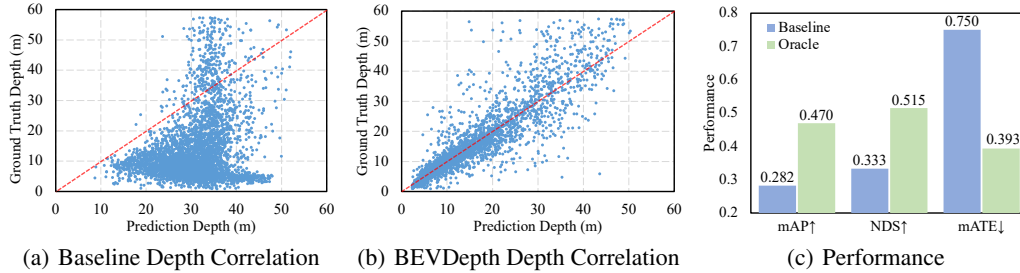


Figure 1: Empirical analysis on the depth correlation and corresponding performances. All experiments are evaluated on nuScenes *val* set. (a) and (b) reveal the depth correlation between ground truth and predicted depth distribution on the baseline model and BEVDepth. (c) indicates the performance of baseline and oracle detector that leverages ground-truth depth.

- The final detection loss encourages the intermediate layer of the network to output the correct depth, establishing an implicit depth supervision. However, deep neural networks typically have complex representations [4]. Without explicit depth supervision, it is challenging for the network to output the depth-aware features accurately.
- The depth sub-network should theoretically be aware of the camera information to correctly deduce the depth from images. Existing methods, however, are blind to camera parameters, leading to inferior results.
- The speed of depth-based 3D detectors is empirically slower than depth-free detectors like FCOS3D [5] when using the same image resolution and backbone, because the view-transform sub-network that comes after depth estimation suffers from extremely poor efficiency.

We present BEVDepth, which introduces an effective sub-network to enable a trustworthy depth estimation, as a solution to these issues. We provide depth supervision that leverages sparse depth data from a point cloud. A Depth Correction module is additionally proposed to align with the perturbed depth ground-truth taking into account the extrinsic disturbance in the movement. To further enable network awareness of camera parameters when predicting depth, a camera-aware attention module is incorporated. Meanwhile, we design a Voxel Pooling operation to quickly project the image feature into BEV, which significantly reduces the cost of the view-transform while consuming the depth.

We are able to detect 3D objects accurately and effectively by combining the aforementioned techniques. Besides, BEVDepth can be easily extended with multi-frame’s inputs by aligning the pseudo point clouds. To verify the efficacy and efficiency of BEVDepth, extensive experiments are carried out. Without any bells and whistles, we achieve 60% NDS on nuScenes test-set.

In conclusion, the following are our main contributions.

- We propose BEVDepth, a multi-view 3D object detector with explicit depth supervision, which simultaneously encodes the camera parameters and disturbance.
- We design a new view-transform operation (namely Efficient Voxel Pooling) to consume the depth, which significantly reduces the time cost.
- We evaluate the proposed BEVDepth on the challenging benchmark nuScenes [6] and achieve state-of-the-art while maintaining the high efficiency.

2 Related Work

2.1 Vision-based 3D object detection

The goal of vision-based 3D detection is to predict the 3D bounding boxes of objects. It is an ill-posed problem because estimating the depth of objects from monocular images is inherently ambiguous. Even when multi-view cameras are available, estimating depth in areas without overlapping views remains challenging. Therefore, depth modeling is a critical component of vision-based 3D detection.

One branch of research predicts 3D bounding boxes directly from 2D image features. 2D detectors, such as CenterNet [7], can be used for 3D detection with minor changes to detection heads. M3D-RPN [8] proposes depth-aware convolutional layers to enhance spatial awareness. D⁴LCN [9] employs depth maps to guide dynamic kernel learning. By converting 3D targets into the image domain, FCOS3D [5] predicts 2D and 3D attributes of objects. Further, PGD [10] presents geometric relation graphs to facilitate depth estimation for 3D object detection. DD3D [11] demonstrates that depth pre-training can significantly improve end-to-end 3D detection.

Another line of work predicts objects in 3D space. There are many ways to convert 2D image features into 3D space. One typical approach is transforming image-based depth maps to pseudo-LiDAR to mimic the LiDAR signal [12, 13, 14]. Image features can also be used to generate 3D voxels [15] or orthographic feature maps [16]. LSS [3] proposes a view transform method that explicitly predicts depth distribution and projects image features onto bird’s-eye view (BEV), which has been proved practical for 3D object detection [2, 1, 17]. BEVFormer [18] performs 2D-to-3D transformation with local attention and grid-shaped BEV queries. Following DETR [19], DETR3D [20] detects 3D objects with transformers and object queries, and PETR [21] improves performance further by introducing 3D position-aware representations.

2.2 LiDAR-based 3D object detection

Due to the accuracy of depth estimation, LiDAR-based 3D detection methods are frequently employed in autonomous driving perception tasks. VoxelNet [22] voxelizes the point cloud, converting it from sparse to dense voxels, and then proposes bounding boxes in dense space to aid the index during convolution. SECOND [23] increases performance on the KITTI dataset [24] by introducing a more effective structure and gt-sampling technique based on VoxelNet [22]. Sparse convolution is also used in SECOND [23] to boost speed. PointPillars [25] encodes point clouds using pillars rather than 3D convolution processes, making it fast but maintaining good performance. CenterPoint [26] proposes an anchor-free detector that extends CenterNet [7] to 3D space and achieves high performance on nuScenes dataset [6] and Waymo open dataset [27]. PointRCNN [28], unlike the grid-based approaches discussed above, creates proposals directly from point clouds. It then employs LiDAR segmentation to identify foreground points for proposals and produce bounding boxes in the second stage. Qi et al. [29] use Hough voting to collect point features and then propose bounding boxes from clusters. Because of its dense feature representation, grid-based approaches are faster, but they lose information from raw point clouds, whereas point-based methods can connect raw point clouds but are inefficient when locating neighbors for each point. PV-RCNN [30] is proposed by Shi et al. to preserve efficiency while allowing adjustable receptive fields for point features.

2.3 Depth Estimation

Depth prediction is critical for monocular image interpretation. Fu et al. [31] employ a regression method to predict the depth of an image using dilated convolution and a scene understanding module. Monodepth [32] predicts depth without supervision using disparity and reconstruction. Monodepth2 [33] uses a combination of depth estimation and pose estimation networks to forecast depth in a single frame.

Some approaches predict depth by constructing cost-volume. MVSNet [34] first introduced cost-volume to the field of depth estimation. Based on MVSNet [34], RMVSNet [35] uses GRU to reduce memory cost, MVSCRF [36] adds CRF module, cascade MVSNet [37] Change MVSNet to cascade structure. Wang et al. [38] generate depth prediction using multi-scale fusion and introduce adaptive modules which improve performance and reduce memory consumption at the same time. Li et al. [39] fuse single-view images with multi-view images and introduce depth-sampling to reduce the cost of computation.

3 BEVDepth

We propose robust Explicit Depth Supervision via Depth Correction and Camera-aware Depth Prediction to enhance intermediate depth, and propose Efficient Voxel Pooling to further speed BEVDepth up. Before getting into the specifics of our innovations, we first elaborate BEVDepth’s overall architecture.

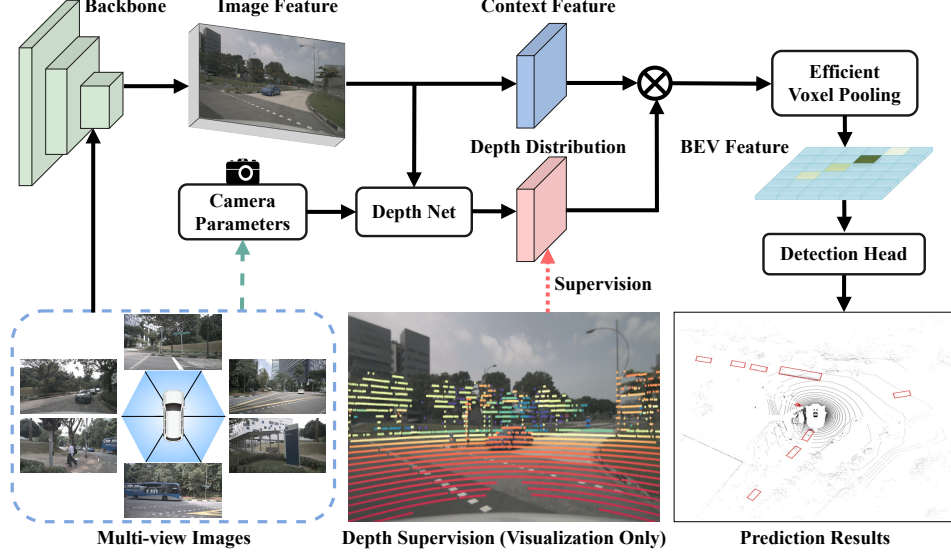


Figure 2: Framework of BEVDepth. Image backbone extracts image feature from multi-view images. Depth net takes Image feature as input, generates context and depth, and gets the final point feature. Voxel Pooling unifies all point features into one coordinate system and pools them onto the BEV feature map.

Overall Architecture Let us start from a vanilla BEVDepth, which simply replaces the segmentation head in LSS [3] with CenterPoint [26] head for 3D detection. It consists of four main components shown in Fig. 2. 1) An Image Encoder (e.g., ResNet [40]) that extracts 2D features $F^{2d} = \{F_i^{2d} \in \mathbb{R}^{C_F \times H \times W}, i = 1, 2, \dots, N\}$ from N view input images $I = \{I_i, i = 1, 2, \dots, N\}$, where H , W and C_F stand for feature’s height, width and channel number; 2) A DepthNet that estimates images depth $D^{pred} = \{D_i^{pred} \in \mathbb{R}^{C_D \times H \times W}, i = 1, 2, \dots, N\}$ from image features F^{2d} , where C_D stands for the number of depth bins; 3) A View Transformer that projects F^{2d} in 3D representations F^{3d} using Eq. 1 then pools them into an integrated BEV representation F^{bev} ; 4) A 3D Detection Head predicting the class, 3D box offset and other attributes.

$$F_i^{3d} = F_i^{2d} \otimes D_i^{pred}, \quad F_i^{3d} \in \mathbb{R}^{C_F \times C_D \times H \times W}. \quad (1)$$

Explicit Depth Supervision In vanilla BEVDepth, the only supervision to the depth module comes from the detection loss. However, due to the difficulty of monocular depth estimation, a sole detection loss is far from enough to supervise the depth module. Therefore, we propose to supervise the intermediate depth prediction D^{pred} using ground-truth D^{gt} derived from point clouds data P . Denote $R_i \in \mathbb{R}^{3 \times 3}$ and $\mathbf{t}_i \in \mathbb{R}^3$ as the rotation and translation matrix from the ego coordinate to the camera coordinate of the i^{th} view, and denote $K_i \in \mathbb{R}^{3 \times 3}$ as the i^{th} camera’s intrinsic parameter. To obtain D^{gt} , we first calculate:

$$P_i^{img}(ud, vd, d) = K_i(R_i P + \mathbf{t}_i), \quad (2)$$

which can be further converted to 2.5D image coordinates $P_i^{img}(u, v, d)$, where u and v denote coordinates in pixel coordinate. If the 2.5D projection of a certain point cloud does not fall into the i^{th} view, we simply discard it. See Fig. 2 for an example of the projection result. Then, to align the shape between the projected point clouds and the predicted depth, a *min pooling* and a *one hot* are adopted on P_i^{img} . We jointly define these two operations as ϕ , the resulting D^{gt} can thus be written in Eq. 3. As for the depth loss L_{depth} , we simply adopt Binary Cross Entropy.

$$D_i^{gt} = \phi(P_i^{img}). \quad (3)$$

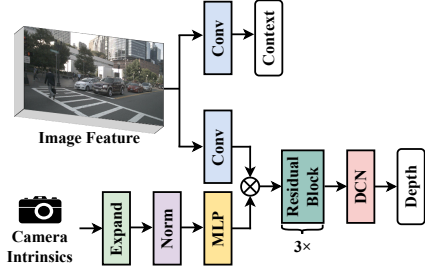


Figure 3: Framework of the depth network. Context feature is generated directly from image feature while a variant of SE-like layer is designed to aggregate with image feature for better estimating the depth.

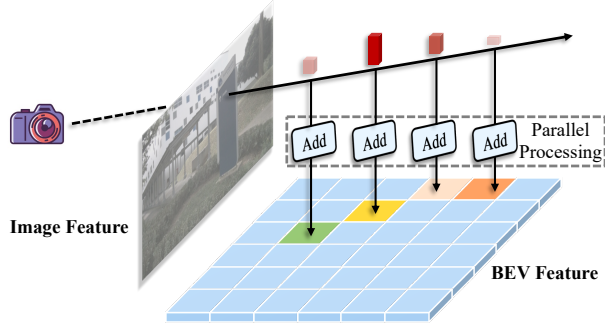


Figure 4: Details of general Efficient Voxel Pooling. For each point, each thread adds the associated point feature to the corresponding position of the BEV feature, and each point corresponds to a thread.

Depth Correction With the help of depth supervision, DepthNet should be able to produce reliable D^{pred} . The calibrated camera parameters R and t may be imprecise at times due to the ego vehicle’s vigorous movement, resulting in spatial mis-alignment between F^{2d} and D^{gt} . The mis-alignment issue becomes more problematic when the DepthNet’s receptive field is constrained. We thus propose a Depth Correction module to alleviate this issue. Instead of adjusting D^{gt} based on ego vehicle’s disturbance, Depth Correction, on the other hand, resolves the mis-alignment issue via increasing the receptive field of DepthNet. Concretely, we stack multiple Residual Blocks [40] in DepthNet, followed by a Deformable Conv [41] as shown in Fig. 3. Benefiting from the improvement of receptive field, the mis-aligned depth gt is able to attend to the feature at right position.

Camera-aware Depth Prediction Above designs improve the model’s ability for depth prediction. However, according to the classic Camera Model, estimating pixel depth is associated to the camera intrinsics, implying that it is non-trivial to model the camera intrinsics into DepthNet. This is especially important in multi-view 3D datasets when cameras may have different FOVs (e.g., nuScenes Dataset [6]). Therefore, to improve the quality of estimated depths D^{pred} , we propose to utilize the camera intrinsics as one of the inputs for DepthNet. Concretely, camera intrinsics’ dimension is first scaled up to the feature’s using an MLP layer. Then, they are used to re-weight the image feature F_i^{2d} with an Squeeze-and-Excitation [42] module. Finally, we concatenate the camera extrinsics to its intrinsics to help DepthNet aware of F^{2d} ’s spatial location in the ego coordinate system. Denote ψ as the original DepthNet, the overall Camera-awareness depth prediction can be written in:

$$D_i^{pred} = \psi(SE(F_i^{2d} | MLP(\xi(R_i) \oplus \xi(t_i) \oplus \xi(K_i))))), \quad (4)$$

where ξ denotes the Flatten operation. An existing work [43] also leverages camera-awareness. They scale the regression targets according to cameras’ intrinsics, making their method hard to adapt to automated systems with complex camera setups. Our method, on the other hand, models the cameras’ parameters inside of the DepthNet, aiming at improving the intermediate depths’ quality. Benefiting from the decoupled nature of LSS [3], the camera-aware depth prediction module is isolated from the detection head and thus the regression target in this case does not need to be changed, resulting in greater extensibility.

Efficient Voxel Pooling Voxel Pooling, aiming at aggregating multi-view features F^{3d} into an integrated BEV feature F^{bev} , is crucial to BEV detectors. In general, it divides the ego space into several evenly distributed grids, and then sums up frustum features that fall into the same grid to form the corresponding BEV feature. To do this, LSS [3] leverages a “cumsum trick” that sorts all frustum features according to their corresponding BEV grid IDs, performs a cumulative sum over all features, then subtracts the cumulative sum values at the boundaries of the bin sections [3]. Such an implementation brings a lot of extra computations since it involves a sorting process over a large amount of BEV coordinates. Moreover, the Prefix Sum adopted by this trick unefficiently runs in a sequential manner. Both deficiencies will harm detector’s overall running speed. One may choose to speed up Prefix Sum by increasing its parallelism, whereas in this work, we introduce a better but

Table 1: Ablation study of depth loss, Depth Correction and Camera-awareness on the nuScenes [6] *val* set. DL denotes Depth Loss, DC denotes Depth Correction and CA denotes Camera-awareness.

DL	DC	CA	mAP \uparrow	mATE \downarrow	mASE \downarrow	mAOE \downarrow	mAVE \downarrow	mAAE \downarrow	NDS \uparrow
			0.282	0.781	0.280	0.671	1.070	0.348	0.333
✓			0.296	0.755	0.277	0.667	1.130	0.357	0.342
✓	✓		0.303	0.725	0.277	0.647	1.108	0.310	0.355
✓	✓	✓	0.315	0.702	0.271	0.621	1.042	0.315	0.367

Table 2: Evaluation of depth prediction on the nuScenes [6] *val* set. DL denotes Depth Loss, DC denotes Depth Correction and CA denotes Camera-awareness.

DL	DC	CA	SILog \downarrow	Abs Rel \downarrow	Sq Rel \downarrow	log10 \downarrow	RMSE \downarrow
			36.884	1.329	29.044	0.304	17.162
✓			22.461	0.335	5.089	0.119	8.968
✓	✓		20.460	0.259	3.623	0.102	8.143
✓	✓	✓	19.802	0.192	2.784	0.097	8.134

much simpler solution that fully leverages the great parallelism of GPU devices, named Efficient Voxel Pooling. As illustrated in Fig. 4, our main idea is to assign each frustum feature a CUDA thread which is used to add that feature to its corresponding BEV grid. As we will illustrate in Sec. 4.2, replacing the original Voxel Pooling operation with our improved version can speed up BEVDepth up to $\times 3$.

4 Experiment

In this section, we first introduce our experimental setups. Then, heavy experiments are conducted to validate the effects of our proposed components. Comparisons with other leading camera 3D detection models are presented in the end.

4.1 Experimental Setup

Dataset and Metrics nuScenes [6] dataset is a large-scale autonomous driving benchmark containing data from six cameras, one LiDAR, and five radars. There are 1000 scenarios in the dataset, which are divided into 700, 150, and 150 scenes for training, validation and testing, respectively. For 3D detection task, we report nuScenes Detection Score (NDS), mean Average Precision (mAP), as well as five True Positive (TP) metrics including mean Average Translation Error (mATE), mean Average Scale Error (mASE), mean Average Orientation Error (mAOE), mean Average Velocity Error (mAVE), mean Average Attribute Error (mAAE). For depth estimation task, we follow the standard evaluation protocol of the prior work [44], reporting scale invariant logarithmic error (SILog), mean absolute relative error (Abs Rel), mean squared relative error (Sq Rel), mean log10 error (log10) and root mean squared error (RMSE) to evaluate our methods.

Implementation Details Unless otherwise specified, we use ResNet-50 [40] as the image backbone and the image size is processed to 256×704 . Following [1], we adopt image data augmentations including random cropping, random scaling, random flipping and random rotation, and also adopt BEV data augmentations including random scaling, random flipping and random rotation. We use AdamW [45] as optimizer with learning rate set to $2e-4$ and batch size set to 64. For ablation study, all experiments are trained for 24 epochs without using CBGS strategy [46]. When comparing to other methods, BEVDepth is trained for 20 epochs with CBGS. Camera-aware DepthNet is placed at the feature level with stride 16.

4.2 Ablation Study

Explicit Depth Supervision and Depth Correction As shown in Tab. 1, our vanilla BEVDepth achieves 28.2% mAP and 33.3% NDS. While obtaining reasonable results, its corresponding depth

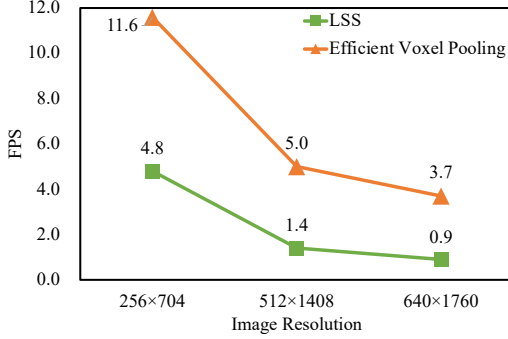


Figure 5: FPS comparison of the whole pipeline using different Voxel Pooling operations.

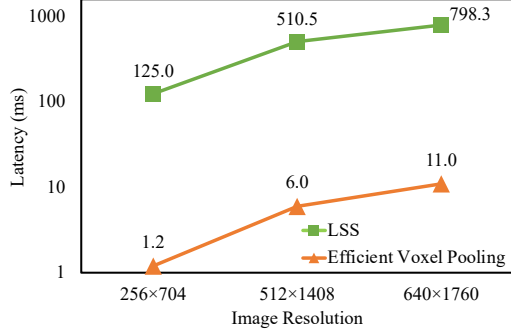


Figure 6: Latency comparison on Voxel Pooling operations only.

Table 3: Ablation study of multi-frame on the nuScenes [6] *val* set. MF denotes multi-frame.

Backbone	Resolution	MF	mAP \uparrow	mATE \downarrow	mASE \downarrow	mAOE \downarrow	mAVE \downarrow	mAAE \downarrow	NDS \uparrow
R50	256×704		0.315	0.702	0.271	0.621	1.042	0.315	0.367
	256×704	✓	0.330	0.699	0.281	0.545	0.493	0.212	0.442
R101	256×704		0.320	0.682	0.272	0.562	0.997	0.284	0.381
	256×704	✓	0.340	0.684	0.273	0.525	0.437	0.231	0.455
R101	512×1408		0.376	0.659	0.267	0.543	1.059	0.335	0.408
	512×1408	✓	0.396	0.635	0.267	0.465	0.434	0.212	0.497

estimation performance in Tab. 2 is surprisingly poor, merely getting 1.33 Abs Rel. Such a result indicates that without depth loss, the learned implicit depth is far from the true value. Compared with baseline, adding depth supervision and Depth Correction module boosts the performance in mAP and NDS by more than 2%. Moreover, mATE is reduced from 0.76 to 0.73. It is worth noting that mATE is related to the depth quality of the predicted 3D objects. We also evaluate our method using depth estimation metrics. As shown in Tab. 2. Using Explicit Depth Supervision and Depth Correction progressively improves the depth quality on all metrics. For example, the Abs Rel is substantially reduced from 1.33 to 0.26. Both the results on detection and depth estimation metrics demonstrate the effectiveness of our proposed modules on depth.

Camera-awareness After adding depth supervision and the Depth Correction module, we proceed to verify the effectiveness of the camera parameter encoding. As shown in Tab.1, the improvements in mAP and mATE reveal that the camera’s parameters are useful for the Depth Estimation module, and that encoding these parameters into the depth module will enhance performance greatly. The improvements on depth metrics in Tab. 2 also lead to the same conclusion.

Efficient Voxel Pooling We compare our Efficient Voxel Pooling with Voxel Pooling in LSS [3] in terms of FPS and latency. Two different resolutions for the input image are adopted: 256×704 and 512×1408. We test on Tesla V100 with a batch size of one. Before applying Efficient Voxel Pooling, the model can run in 11.6 frames/second and 3.7 frames/second respectively for small and large resolution input images. The FPS of the pipeline after employing Efficient Voxel Pooling is four times that of the pipeline without Efficient Voxel Pooling under the large resolution of the input image as shown in Fig. 5. As an empirical result, the training time of large resolution input can be reduced from 5 days to 1.5 days in our experiments. We also test the latency of the single module in Fig. 6, showing that Efficient Voxel Pooling is 80 times faster than LSS.

Multi-frame Fusion Multi-frame Fusion scheme is generally adopted in LiDAR-based detectors [26, 25, 23], since it is beneficial to identifying objects and improving the velocity estimation ability. Inspired by FlowNet [47], we fuse two frames by directly concatenating their BEV features. However, due to the existence of ego-motion, direct fusion may cause spatial mis-alignment. We notice that LSS-based detectors usually leverage pseudo point clouds F^{3d} as intermediate features. It is natural and efficient to align pseudo point clouds before Voxel Pooling. Concretely, for each point $\mathcal{P}^{\text{prev}}$ at a previous timestamp, we first convert it into coordinate system at the current timestamp by:

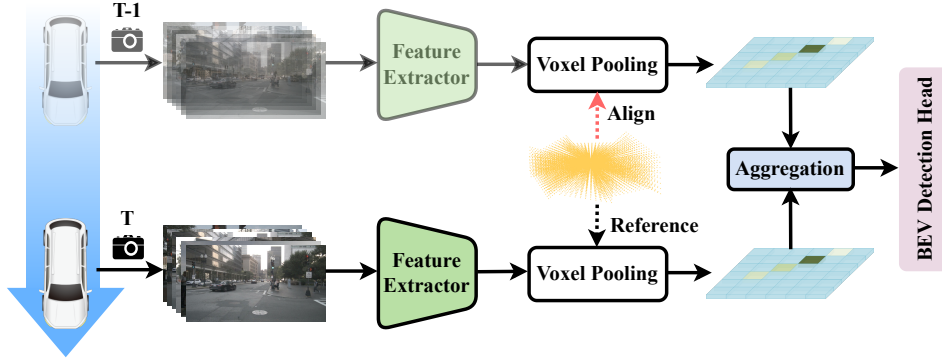


Figure 7: Pipeline of sequence modeling. It first aligns the history point cloud into current state with ego pose. Then pooling the pseudo point cloud to BEV feature for aggregation. Finally, the BEV detection head is attached to predict better results.

Table 4: Comparison on the nuScenes *val* set. L denotes LiDAR and C denotes camera.

Method	Resolution	Modality	mAP \uparrow	mATE \downarrow	mASE \downarrow	mAOE \downarrow	mAVE \downarrow	mAAE \downarrow	NDS \uparrow
CenterPoint-Voxel [26]	-	L	0.564	-	-	-	-	-	0.648
CenterPoint-Pillar	-	L	0.503	-	-	-	-	-	0.602
FCOS3D [5]	900 \times 1600	C	0.295	0.806	0.268	0.511	1.315	0.170	0.372
DETR3D [20]	900 \times 1600	C	0.303	0.860	0.278	0.437	0.967	0.235	0.374
BEVDet-R50 [1]	256 \times 704	C	0.286	0.724	0.278	0.590	0.873	0.247	0.372
BEVDet-Base	512 \times 1408	C	0.349	0.637	0.269	0.490	0.914	0.268	0.417
PETR-R50 [21]	384 \times 1056	C	0.313	0.768	0.278	0.564	0.923	0.225	0.381
PETR-R101	512 \times 1408	C	0.357	0.710	0.270	0.490	0.885	0.224	0.421
PETR-Tiny	512 \times 1408	C	0.361	0.732	0.273	0.497	0.808	0.185	0.431
BEVDet4D-Tiny [17]	256 \times 704	C	0.323	0.674	0.272	0.503	0.429	0.208	0.453
BEVDet4D-Base	640 \times 1600	C	0.396	0.619	0.260	0.361	0.399	0.189	0.515
BEVFormer-S [18]	-	C	0.375	0.725	0.272	0.391	0.802	0.200	0.448
BEVFormer-R101-DCN	900 \times 1600	C	0.416	0.673	0.274	0.372	0.394	0.198	0.517
BEVDepth-R50	256 \times 704	C	0.351	0.639	0.267	0.479	0.428	0.198	0.475
BEVDepth-R101	512 \times 1408	C	0.412	0.565	0.266	0.358	0.331	0.190	0.535

$$\mathcal{P}^{\text{cur}} = \mathcal{T}^{\text{global2cur}} \cdot \mathcal{T}^{\text{prev2global}} \cdot \mathcal{P}^{\text{prev}}, \quad (5)$$

where \mathcal{T} denotes translation-rotation matrix. We then use aligned coordinates to execute Voxel Pooling on pseudo point clouds, resulting in aligned BEV features for historical and present timestamps. Finally, all of the features are combined and applied to the final detection.

We still use 256 \times 704 and 512 \times 1408 resolution as input resolutions. Tab. 3 shows that the multi-frame scheme substantially reduces mAVE *e.g.*, from 1.04 to 0.49 on ResNet-50. The NDS and mAAE are correspondingly improved. Meanwhile, mAP on ResNet-50 is also improved from 31.5% to 33.0%. Based on the aforementioned analysis, we can conclude that our Multi-frame Fusion approach enables the model to sense the object’s velocity and enhances model’s capability on recognizing objects.

4.3 Benchmark Results

nuScenes val set We compare the proposed BEVDepth with other state-of-the-art methods like FCOS3D [5], DETR3D [20], BEVDet [1], PETR [21], BEVDet4D [17] and BEVFormer [18] on nuScenes [6] val set. We don’t adopt test time augmentation. As can be seen from Tab. 4, BEVDepth shows superior performance in mATE and NDS (a key metric of nuScenes dataset), which improves 5% and 2% over 2nd place, respectively. BEVDepth is also comparable with BEVFormer in mAP given the fact that they use stronger backbone and larger resolution input images. Using 256 \times 704 resolution input images, BEVDepth exceeds BEVDet on ResNet-50 by 10% in NDS. BEVDepth also exceeds BEVDet4D-Tiny and BEVFormer-S by 2% in NDS. When using 512 \times 1408 resolution

Table 5: Comparison on the nuScenes *test* set. L denotes LiDAR and C denotes camera.

Method	Modality	mAP \uparrow	mATE \downarrow	mASE \downarrow	mAOE \downarrow	mAVE \downarrow	mAAE \downarrow	NDS \uparrow
CenterPoint [26]	L	0.674	0.255	0.235	0.339	0.233	0.128	0.718
FCOS3D [5]	C	0.358	0.690	0.249	0.452	1.434	0.124	0.428
DETR3D [20]	C	0.412	0.641	0.255	0.394	0.845	0.133	0.479
BEVDet-Pure [1]	C	0.398	0.556	0.239	0.414	1.010	0.153	0.463
BEVDet-Beta	C	0.422	0.529	0.236	0.396	0.979	0.152	0.482
PETR [21]	C	0.434	0.641	0.248	0.437	0.894	0.143	0.481
PETR-e	C	0.441	0.593	0.249	0.384	0.808	0.132	0.504
BEVDet4D [17]	C	0.451	0.511	0.241	0.386	0.301	0.121	0.569
BEVFormer [18]	C	0.481	0.582	0.256	0.375	0.378	0.126	0.569
BEVDepth	C	0.503	0.445	0.245	0.378	0.320	0.126	0.600

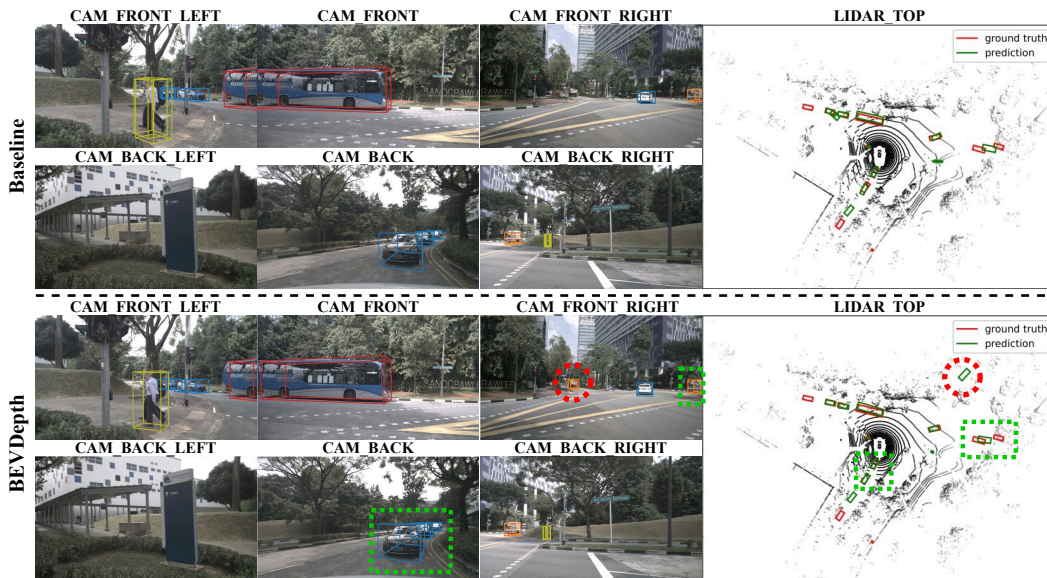


Figure 8: Comparison of baseline and BEVDepth. We use the green dotted rectangle to mark the samples that BEVDepth yields more accurate localization results. The red dotted circle indicates the sample that is missed by the baseline and GT, but still detected by our method.

input images, BEVDepth exceeds PETR on ResNet-101 6% in mAP, 0.14 in mATE and 11% in NDS. BEVDepth also exceeds BEVDET4D-Base 2% in mAP, 0.05 in mATE and 2% in NDS although their backbones are usually better than us.

nuScenes test set For the submitted results on the test set, we use the train set and val set for training. The result we submitted is a single model with test time augmentation. As listed in Tab.5, BEVDepth ranks first on the nuScenes camera 3D objection leader board with a score of 50.3% mAP and 60% NDS. On mAP, we outperform the past two best methods BEVDet4D and BEVFormer by 5% and 2%, respectively. On mATE, a key metric reflecting depth prediction accuracy, we outperform these two methods by 7% and 13%, respectively. On NDS, we surpass the second place by 3%, and on other metrics, we remain at or on par with the best methods in the past.

4.4 Visualization

As shown in Fig. 8, we present results in camera space and BEV space. From the samples marked by green rectangles, we can see that our BEVDepth performs better than the baseline method in terms of

the BEV localization. Moreover, the sample marked by red circle is not annotated but still detected by our method, demonstrating BEVDepth’s capability on detecting objects from far distance.

5 Conclusion

In this paper, a novel network architecture, namely BEVDepth, is proposed for accurate depth prediction in the 3D object detection task. By introducing Depth Correction module with depth supervision, BEVDepth is able to perceive camera disturbance and generate robust depth prediction. BEVDepth obtains the capacity to predict trustworthy depth by combining visual attributes with camera specifications. BEVDepth additionally use the Point-based Frame Fusion schema to enrich information in the current frame by fusing data from previous frames, which is useful for predicting velocity and depth. In addition, we propose Efficient Voxel Pooling, which completely avoids index sorting and take advantage of GPU parallelism. Experimental results on nuScenes demonstrate its effectiveness and potential in practical applications.

References

- [1] Junjie Huang, Guan Huang, Zheng Zhu, and Dalong Du. Bevdet: High-performance multi-camera 3d object detection in bird-eye-view. *arXiv preprint arXiv:2112.11790*, 2021.
- [2] Cody Reading, Ali Harakeh, Julia Chae, and Steven L Waslander. Categorical depth distribution network for monocular 3d object detection. In *Proceedings of the IEEE/CVF Conference on Computer Vision and Pattern Recognition*, pages 8555–8564, 2021.
- [3] Jonah Philion and Sanja Fidler. Lift, splat, shoot: Encoding images from arbitrary camera rigs by implicitly unprojecting to 3d. In *European Conference on Computer Vision*, pages 194–210. Springer, 2020.
- [4] Matthew D Zeiler and Rob Fergus. Visualizing and understanding convolutional networks. In *European conference on computer vision*, pages 818–833. Springer, 2014.
- [5] Tai Wang, Xinge Zhu, Jiangmiao Pang, and Dahua Lin. Fcos3d: Fully convolutional one-stage monocular 3d object detection. In *Proceedings of the IEEE/CVF International Conference on Computer Vision*, pages 913–922, 2021.
- [6] Holger Caesar, Varun Bankiti, Alex H Lang, Sourabh Vora, Venice Erin Liong, Qiang Xu, Anush Krishnan, Yu Pan, Giancarlo Baldan, and Oscar Beijbom. nuscenes: A multimodal dataset for autonomous driving. In *Proceedings of the IEEE/CVF conference on computer vision and pattern recognition*, pages 11621–11631, 2020.
- [7] Xingyi Zhou, Dequan Wang, and Philipp Krähenbühl. Objects as points. *arXiv preprint arXiv:1904.07850*, 2019.
- [8] Garrick Brazil and Xiaoming Liu. M3d-rpn: Monocular 3d region proposal network for object detection. In *Proceedings of the IEEE/CVF International Conference on Computer Vision*, pages 9287–9296, 2019.
- [9] Yuqi Huo, Hongwei Yi, Zhe Wang, Jianping Shi, Zhiwu Lu, Ping Luo, et al. Learning depth-guided convolutions for monocular 3d object detection. In *2020 IEEE/CVF Conference on Computer Vision and Pattern Recognition Workshops (CVPRW)*, pages 4306–4315. IEEE, 2020.
- [10] Tai Wang, ZHU Xinge, Jiangmiao Pang, and Dahua Lin. Probabilistic and geometric depth: Detecting objects in perspective. In *Conference on Robot Learning*, pages 1475–1485. PMLR, 2022.
- [11] Dennis Park, Rares Ambrus, Vitor Guizilini, Jie Li, and Adrien Gaidon. Is pseudo-lidar needed for monocular 3d object detection? In *Proceedings of the IEEE/CVF International Conference on Computer Vision*, pages 3142–3152, 2021.
- [12] Yan Wang, Wei-Lun Chao, Divyansh Garg, Bharath Hariharan, Mark Campbell, and Kilian Q Weinberger. Pseudo-lidar from visual depth estimation: Bridging the gap in 3d object detection for autonomous driving. In *Proceedings of the IEEE/CVF Conference on Computer Vision and Pattern Recognition*, pages 8445–8453, 2019.
- [13] Yurong You, Yan Wang, Wei-Lun Chao, Divyansh Garg, Geoff Pleiss, Bharath Hariharan, Mark Campbell, and Kilian Q Weinberger. Pseudo-lidar++: Accurate depth for 3d object detection in autonomous driving. *arXiv preprint arXiv:1906.06310*, 2019.
- [14] Rui Qian, Divyansh Garg, Yan Wang, Yurong You, Serge Belongie, Bharath Hariharan, Mark Campbell, Kilian Q Weinberger, and Wei-Lun Chao. End-to-end pseudo-lidar for image-based 3d object detection. In *Proceedings of the IEEE/CVF Conference on Computer Vision and Pattern Recognition*, pages 5881–5890, 2020.

- [15] Danila Rukhovich, Anna Vorontsova, and Anton Konushin. Imvoxelnet: Image to voxels projection for monocular and multi-view general-purpose 3d object detection. In *Proceedings of the IEEE/CVF Winter Conference on Applications of Computer Vision*, pages 2397–2406, 2022.
- [16] Thomas Roddick, Alex Kendall, and Roberto Cipolla. Orthographic feature transform for monocular 3d object detection. *arXiv preprint arXiv:1811.08188*, 2018.
- [17] Junjie Huang and Guan Huang. Bevdet4d: Exploit temporal cues in multi-camera 3d object detection. *arXiv preprint arXiv:2203.17054*, 2022.
- [18] Zhiqi Li, Wenhai Wang, Hongyang Li, Enze Xie, Chonghao Sima, Tong Lu, Qiao Yu, and Jifeng Dai. Bevformer: Learning bird’s-eye-view representation from multi-camera images via spatiotemporal transformers. *arXiv preprint arXiv:2203.17270*, 2022.
- [19] Nicolas Carion, Francisco Massa, Gabriel Synnaeve, Nicolas Usunier, Alexander Kirillov, and Sergey Zagoruyko. End-to-end object detection with transformers. In *European conference on computer vision*, pages 213–229. Springer, 2020.
- [20] Yue Wang, Vitor Campagnolo Guizilini, Tianyuan Zhang, Yilun Wang, Hang Zhao, and Justin Solomon. Detr3d: 3d object detection from multi-view images via 3d-to-2d queries. In *Conference on Robot Learning*, pages 180–191. PMLR, 2022.
- [21] Yingfei Liu, Tiancai Wang, Xiangyu Zhang, and Jian Sun. Petr: Position embedding transformation for multi-view 3d object detection. *arXiv preprint arXiv:2203.05625*, 2022.
- [22] Yin Zhou and Oncel Tuzel. Voxelnet: End-to-end learning for point cloud based 3d object detection. In *Proceedings of the IEEE conference on computer vision and pattern recognition*, pages 4490–4499, 2018.
- [23] Yan Yan, Yuxing Mao, and Bo Li. Second: Sparsely embedded convolutional detection. *Sensors*, 18(10):3337, 2018.
- [24] Andreas Geiger, Philip Lenz, and Raquel Urtasun. Are we ready for autonomous driving? the kitti vision benchmark suite. In *2012 IEEE conference on computer vision and pattern recognition*, pages 3354–3361. IEEE, 2012.
- [25] Alex H Lang, Sourabh Vora, Holger Caesar, Lubing Zhou, Jiong Yang, and Oscar Beijbom. Pointpillars: Fast encoders for object detection from point clouds. In *Proceedings of the IEEE/CVF Conference on Computer Vision and Pattern Recognition*, pages 12697–12705, 2019.
- [26] Tianwei Yin, Xingyi Zhou, and Philipp Krahenbuhl. Center-based 3d object detection and tracking. In *Proceedings of the IEEE/CVF conference on computer vision and pattern recognition*, pages 11784–11793, 2021.
- [27] Pei Sun, Henrik Kretzschmar, Xerxes Dotiwalla, Aurelien Chouard, Vijaysai Patnaik, Paul Tsui, James Guo, Yin Zhou, Yuning Chai, Benjamin Caine, et al. Scalability in perception for autonomous driving: Waymo open dataset. In *Proceedings of the IEEE/CVF conference on computer vision and pattern recognition*, pages 2446–2454, 2020.
- [28] Shaoshuai Shi, Xiaogang Wang, and Hongsheng Li. Pointcnn: 3d object proposal generation and detection from point cloud. In *Proceedings of the IEEE/CVF conference on computer vision and pattern recognition*, pages 770–779, 2019.
- [29] Charles R Qi, Or Litany, Kaiming He, and Leonidas J Guibas. Deep hough voting for 3d object detection in point clouds. In *proceedings of the IEEE/CVF International Conference on Computer Vision*, pages 9277–9286, 2019.
- [30] Shaoshuai Shi, Chaoxu Guo, Li Jiang, Zhe Wang, Jianping Shi, Xiaogang Wang, and Hongsheng Li. Pv-rcnn: Point-voxel feature set abstraction for 3d object detection. In *Proceedings of the IEEE/CVF Conference on Computer Vision and Pattern Recognition*, pages 10529–10538, 2020.
- [31] Huan Fu, Mingming Gong, Chaohui Wang, Kayhan Batmanghelich, and Dacheng Tao. Deep ordinal regression network for monocular depth estimation. In *Proceedings of the IEEE conference on computer vision and pattern recognition*, pages 2002–2011, 2018.
- [32] Clément Godard, Oisín Mac Aodha, and Gabriel J Brostow. Unsupervised monocular depth estimation with left-right consistency. In *Proceedings of the IEEE conference on computer vision and pattern recognition*, pages 270–279, 2017.
- [33] Clément Godard, Oisín Mac Aodha, Michael Firman, and Gabriel J Brostow. Digging into self-supervised monocular depth estimation. In *Proceedings of the IEEE/CVF International Conference on Computer Vision*, pages 3828–3838, 2019.
- [34] Yao Yao, Zixin Luo, Shiwei Li, Tian Fang, and Long Quan. Mvsnet: Depth inference for unstructured multi-view stereo. In *Proceedings of the European Conference on Computer Vision (ECCV)*, pages 767–783, 2018.

- [35] Yao Yao, Zixin Luo, Shiwei Li, Tianwei Shen, Tian Fang, and Long Quan. Recurrent mvsnets for high-resolution multi-view stereo depth inference. In *Proceedings of the IEEE/CVF Conference on Computer Vision and Pattern Recognition*, pages 5525–5534, 2019.
- [36] Youze Xue, Jiansheng Chen, Weitao Wan, Yiqing Huang, Cheng Yu, Tianpeng Li, and Jiayu Bao. Mvscrf: Learning multi-view stereo with conditional random fields. In *Proceedings of the IEEE/CVF International Conference on Computer Vision*, pages 4312–4321, 2019.
- [37] Xiaodong Gu, Zhiwen Fan, Siyu Zhu, Zuozhuo Dai, Feitong Tan, and Ping Tan. Cascade cost volume for high-resolution multi-view stereo and stereo matching. In *Proceedings of the IEEE/CVF Conference on Computer Vision and Pattern Recognition*, pages 2495–2504, 2020.
- [38] Fangjinhua Wang, Silvano Galliani, Christoph Vogel, Pablo Speciale, and Marc Pollefeys. Patchmatchnet: Learned multi-view patchmatch stereo. In *Proceedings of the IEEE/CVF Conference on Computer Vision and Pattern Recognition*, pages 14194–14203, 2021.
- [39] Zhaoshuo Li, Xingtong Liu, Nathan Drenkow, Andy Ding, Francis X Creighton, Russell H Taylor, and Mathias Unberath. Revisiting stereo depth estimation from a sequence-to-sequence perspective with transformers. In *Proceedings of the IEEE/CVF International Conference on Computer Vision*, pages 6197–6206, 2021.
- [40] Kaiming He, Xiangyu Zhang, Shaoqing Ren, and Jian Sun. Deep residual learning for image recognition. In *Proceedings of the IEEE conference on computer vision and pattern recognition*, pages 770–778, 2016.
- [41] Xizhou Zhu, Han Hu, Stephen Lin, and Jifeng Dai. Deformable convnets v2: More deformable, better results. In *Proceedings of the IEEE/CVF conference on computer vision and pattern recognition*, pages 9308–9316, 2019.
- [42] Jie Hu, Li Shen, and Gang Sun. Squeeze-and-excitation networks. In *Proceedings of the IEEE conference on computer vision and pattern recognition*, pages 7132–7141, 2018.
- [43] Dennis Park, Rares Ambrus, Vitor Guizilini, Jie Li, and Adrien Gaidon. Is pseudo-lidar needed for monocular 3d object detection? In *Proceedings of the IEEE/CVF International Conference on Computer Vision*, pages 3142–3152, 2021.
- [44] David Eigen, Christian Puhrsch, and Rob Fergus. Depth map prediction from a single image using a multi-scale deep network. *Advances in neural information processing systems*, 27, 2014.
- [45] Ilya Loshchilov and Frank Hutter. Decoupled weight decay regularization. *arXiv preprint arXiv:1711.05101*, 2017.
- [46] Benjin Zhu, Zhengkai Jiang, Xiangxin Zhou, Zeming Li, and Gang Yu. Class-balanced grouping and sampling for point cloud 3d object detection. *arXiv preprint arXiv:1908.09492*, 2019.
- [47] Alexey Dosovitskiy, Philipp Fischer, Eddy Ilg, Philip Hausser, Caner Hazirbas, Vladimir Golkov, Patrick Van Der Smagt, Daniel Cremers, and Thomas Brox. FlowNet: Learning optical flow with convolutional networks. In *Proceedings of the IEEE international conference on computer vision*, pages 2758–2766, 2015.